Nanoscale

RSC Publishing

PAPER

View Article Online
View Journal | View Issue

Cite this: *Nanoscale*, 2013, **5**, 5549

Nano-silica fabricated with silver nanoparticles: antifouling adsorbent for efficient dye removal, effective water disinfection and biofouling control†

Sujoy K. Das,*[a] Md. Motiar R. Khan,[c] T. Parandhaman,[a] Fathima Laffir,[d] Arun K. Guha,[c] G. Sekaran[a] and Asit Baran Mandal*[b]

A nano-silica–AgNPs composite material is proposed as a novel antifouling adsorbent for cost-effective and ecofriendly water purification. Fabrication of well-dispersed AgNPs on the nano-silica surface, designated as NSAgNP, has been achieved through protein mediated reduction of silver ions at ambient temperature for development of sustainable nanotechnology. The coated proteins on AgNPs led to the formation of stable NSAgNP and protected the AgNPs from oxidation and other ions commonly present in water. The NSAgNP exhibited excellent dye adsorption capacity both in single and multicomponent systems, and demonstrated satisfactory tolerance against variations in pH and dye concentration. The adsorption mainly occurred through electrostatic interaction, though π–π interaction and pore diffusion also contributed to the process. Moreover, the NSAgNP showed long-term antibacterial activity against both planktonic cells and biofilms of Gram-negative *Escherichia coli* and *Pseudomonas aeruginosa*. The antibacterial activity of AgNPs retarded the initial attachment of bacteria on NSAgNP and thus significantly improved the antifouling properties of the nanomaterial, which further inhibited biofilm formation. Scanning electron and fluorescence microscopic studies revealed that cell death occurred due to irreversible damage of the cell membrane upon electrostatic interaction of positively charged NSAgNP with the negatively charged bacterial cell membrane. The high adsorption capacity, reusability, good tolerance, removal of multicomponent dyes and *E. coli* from the simulated contaminated water and antifouling properties of NSAgNP will provide new opportunities to develop cost-effective and ecofriendly water purification processes.

Received 18th February 2013
Accepted 8th April 2013

DOI: 10.1039/c3nr00856h

www.rsc.org/nanoscale

Introduction

The Earth's water resources are being increasingly contaminated with rapid industrialization, which recklessly pollutes water-bodies with various organic and inorganic hazardous chemicals.[1] Huge quantities of different types of dyes from the tannery, paint, paper and textile industries that are discharged into the environment are toxic and even carcinogenic, causing a serious environmental threat to aquatic and human life.[2,3] The availability of and access to a clean, secure and sustainable source of pure water is therefore, an urgent need in the present century.[4] Thus, efficient separation and remediation technology is the crying need of the hour for pollution control management.

Various conventional practices such as ion exchange, reverse osmosis, ultrafiltration, oxidation, ozonation, adsorption, *etc.*, have been employed for the treatment of dye-bearing wastewater.[5–7] However, these techniques suffer certain limitations including cost effectiveness, low adsorption capacity or inadequate affinity in removing dye from wastewater. Advances in nanoscience and technology are providing new opportunities to develop cost-effective and environmental benign water purification technologies. Nanostructured adsorbents like mesoporous titania beads, alumina, metal or metal oxides, polyetheleneimine/polyvinyl alcohol nanofibers, *etc.* have recently demonstrated remarkable advancement in this regard due to their higher surface areas and surface active sites.[8–14] However, the application of such types of nanomaterials unavoidably suffers from certain inherent limitations. During the treatment process these materials aggregate very frequently and thus reduce the adsorption efficiency. In addition, in aquatic environments these are prone to fouling (organic fouling, colloidal fouling, and biofouling). Among all types of fouling, biofilm formation on the surface (biofouling) causes

[a]*Environmental Technology Division, Council of Scientific and Industrial Research (CSIR)-Central Leather Research Institute (CLRI), Chennai, India. E-mail: sujoy@clri.res.in; sujoydasiacs@gmail.com; Fax: +91 4424911589; Tel: +91 4424437132*

[b]*Chemical Laboratory, Council of Scientific and Industrial Research (CSIR)-Central Leather Research Institute (CLRI), Chennai, India. E-mail: abmandal@hotmail.com; Fax: +91 4424912150; Tel: +91 4424910846*

[c]*Department of Biological Chemistry, Indian Association for the Cultivation of Science, Kolkata, India*

[d]*Materials and Surface Science Institute, University of Limerick, Ireland*

† Electronic supplementary information (ESI) available: Other experimental details and additional results. See DOI: 10.1039/c3nr00856h

reduction of pore size and surface roughness and blockage of surface functional groups.[15,16] This leads to higher energy consumption, operational expenditure, accelerated corrosion and the generation of antibiotic resistant strains, which create significant health and economic problems.[17,18]

The most effective ways to inhibit biofilm formation is to prevent bacterial adhesion on the surface, which is a critical step of colonization.[18,19] The successive long term operation of wastewater treatment thus requires formation of stable and antifouling nanomaterials which may prevent biofilm formation. Control of bacterial adhesion on nanomaterials by coating with antimicrobial agent is therefore crucial for designing antifouling materials for efficient water treatment processes.[17] Nanoscale silver materials (AgNPs) exhibited broad spectrum antimicrobial activity with low toxicity to mammalian cells.[20–23] Colloidal silver has been approved by the U. S. Environmental Protection Agency as a disinfectant for hospitals and medical centers.[24] Fabrication of AgNPs on a supportive material could offer a potential solution to inhibit biofilm formation. As a potent antibacterial agent, AgNPs may prevent biofouling on nanomaterials and inhibit biofilm formation. In the last few years, numerous methods have been developed to fabricate AgNPs on a large variety of porous supportive materials, like microporous polymers, mesoporous silica, cellulose, carbon nanotubes and nanofibers, *etc.*[21–23,25,26] Impregnation and coprecipitation are mostly adopted for the fabrication of metal nanoparticles on solid supports.[25] In addition, hydrothermal reactions and sol–gel methods have also been used for fabrication of metal nanoparticles.[26] All these chemical methodologies often generate toxic and/or flammable by-products,[27,28] which unavoidably trigger environmental and safety issues. However, the aggregation behavior of AgNPs in aqueous medium often hampers their antimicrobial properties and leaching of silver ions over time leading to a gradual loss in the efficiency as well as causing environmental contamination.[29] In addition, the activities of these porous composite materials decrease due to mass transfer reactions.[30] Therefore, the development of a facile and expedient approach for the synthesis of new stable nanomaterials through fabrication of AgNPs on nonporous material is highly desirable to prevent pore diffusion and biofilm formation.

Inspired by natural biomineralization processes, the biosynthetic route has recently gained significant attention for the design and fabrication of advanced nanostructured materials.[31–34] Numerous efforts have been made utilizing various types of biological molecules such as nucleic acids, proteins, peptide, bacteria, fungi, *etc.*, for synthesizing novel functional nanomaterials, which satisfy many principles of green chemistry.[34–38] Very recently, we have developed a fungal-protein-mediated synthesis of metal nanoparticles.[29,32,36,37] Despite the initial success of *in vitro* biosynthesis of metal nanoparticles, the fabrication of metal nanoparticles on supportive materials through a biomineralization process has yet to be reported.

In this work, a simple, green chemical method has been developed to fabricate protein coated AgNPs on the surface of nano-silica to form a stable functional composite material. This we referred as NSAgNP. The synthesized NSAgNP has been characterized thoroughly and tested as a novel antifouling nanomaterial for efficient removal of dyes and pathogenic microorganisms from water-bodies. Its unique features, such as high surface area, less pore volume, and high surface active sites, boosted not only high adsorption of dyes but also efficiently killed bacteria and prevented biofilm formation. The multiplex dye adsorbability, strong antimicrobial and antifouling properties of the proposed inorganic–organic hybrid nanomaterial may provide a better solution for water treatment technology.

Experimental

Materials

Silver nitrate ($AgNO_3$), Congo red (CR), Eosin yellow (EY), Bromophenol blue (BPB), Brilliant blue (BB) and all other chemicals were purchased from Merck, India. Microbiological ingredients were obtained from HiMedia, India.

Microorganisms

Rhizopus oryzae (MTCC 262), *Escherichia coli* (MTCC 062), and *Pseudomonas aeruginosa* (MTCC 424) were obtained from the Institute of Microbial Technology, Chandigarh, India. The fungal and bacterial strains were maintained on potato dextrose and nutrient agar slants, respectively.

Dye solution

Stock solutions (2000 mg L^{-1}) of (CR), (EY), (BPB), and (BB) were prepared in deionized and double distilled water and diluted to get the desired concentrations of the dyes. Calibration curves of CR (λ_{max} 497 nm), EY (λ_{max} 518 nm), BPB (λ_{max} 484 nm), and BB (λ_{max} 552 nm) were prepared by measuring the absorbance of different concentrations of the dyes using a UV-vis spectrophotometer (Varian CARY 100 Bio). A complex cocktail dye (CD) solution was prepared by mixing all these four dyes in equal amount to a concentration of 50 mg L^{-1}. The maximum absorbance of the CD was set at 595 nm through scanning the solution in UV-vis spectrophotometer. The calibration curve of CD was prepared as described above with varying dye concentrations. The dye concentrations in the experimental samples were calculated from the calibration curves.

Methods

Biosynthesis of nano-silica silver nanomaterial (NSAgNP)

Nano-silica powder (20 mg) was added to 25 mL of $AgNO_3$ solution (1000 mg L^{-1}, pH 6.0) and incubated with shaking (120 rpm) at 30 °C for 2 h. 5 mL protein extract (6 mg mL^{-1}) of *R. oryzae* (see ESI†) was then added to the solution and incubated at 30 °C for another 48 h with shaking. The formation of NSAgNP material was monitored by observing the color change of nano-silica from white to a deep brown color. A control experiment was performed under identical conditions in the absence of protein extract. The as-synthesized NSAgNP was collected by centrifugation (10 000 rpm, 15 min), and dried at 50 °C for 5 h in a hot air oven. The dried NSAgNP was then characterized by UV-vis spectroscopy, X-ray photoelectron

spectroscopy (XPS) and high resolution transmission electron microscopy (HRTEM).

Characterization of NSAgNP

Both control nano-silica and NSAgNP were dispersed in deionized water by sonication and then scanned on a UV-vis spectrophotometer. The samples for HRTEM analysis were prepared by drop-casting an NSAgNP suspension on a copper grid. The images were recorded on a HRTEM (JEOL JEM 2010) operating at an accelerating voltage of 200 kV equipped with an energy dispersive X-ray analysis (EDXA) system. The selected area electron diffraction (SAED) pattern was recorded from HRTEM images to obtain the crystal structure. The crystal planes were analyzed using JCPDS software. The biosynthesis mechanism of NSAgNP formation was studied by X-ray photoelectron spectroscopy (XPS). The spectroscopic measurements were carried out using a high performance X-ray photoelectron spectrometer (Kartos AXIS 165).[32,36] The surface charge of NSAgNP was measured through Zeta potential analysis. The sample (2 mg mL^{-1}) was dispersed in deionized double distilled water and the Zeta potential was measured on a Zetasizer (Malvern Zetasizer).

Adsorption of dyes by NSAgNP material

The NSAgNP was used as an adsorbent for the removal of different anionic and cationic dyes from aqueous solution. The NSAgNP was conditioned at different pH values (2.0–9.0) and used for adsorption of CR, EY, BPB, and BB. The pH values of the suspensions were adjusted by addition of 1 M HCl or NaOH solution, as required. 25 mL of 50 mg L^{-1} CR, EY, BPB, and BB solutions were taken in 100 mL Erlenmeyer flasks separately, and conditioned NSAgNP (2 mg mL^{-1}) was then added to the solution followed by incubation for 24 h under shaking (120 rpm). On completing incubation, the dye solutions were collected by centrifugation (10 000 rpm, 15 min) and the concentrations of the dyes were measured spectrophotometrically as described above. The control experiments were carried out without addition of NSAgNP. The amount of dye adsorbed on the adsorbent was calculated using mass balance equation as described elsewhere.[39]

The four dyes were then mixed together and used for adsorptive removal of this complex cocktail of dyes (CD) using NSAgNP in a similar fashion as described above. The rest of the work was carried out with this mixed cocktail of dyes. The kinetics of CD by NSAgNP was carried out at three different pH values (4.2, 6.8, and 9.1) using 50 mg L^{-1} dye solution. The pH conditioned NSAgNP were added to the dye solution and the concentration of the dye was measured at regular intervals up to 2 h, keeping other experimental conditions constant. The equilibrium adsorption isotherm was conducted as described above using various dye concentrations (10–2000 mg L^{-1}), the pH and temperature of incubation being 6.0 and 30 °C, respectively.

Recycling of NSAgNP material

NSAgNP was collected after dye adsorption and thoroughly washed with deionized and double distilled water. The dye loaded NSAgNP was then transferred to different conical flasks and incubated with 10 mL of HCl (0.1 M), H_2SO_4 (0.1 M), HNO_3 (0.1 M), NaOH (0.1 M) and various organic solvents *viz.* ethanol, methanol and acetone for 1 h with shaking (120 rpm). At the end of the incubation period NSAgNP was collected and the concentration of the eluted dyes in the solution was measured spectrophotometrically. The regenerated NSAgNP was washed with double distilled water, dried and further used for dye adsorption as described above.

Antimicrobial activity of NSAgNP material and biofilm formation inhibition

The bactericidal activity of NSAgNP on *E. coli* and *P. aeruginosa* was determined by plate count method. In brief, *E. coli* and *P. aeruginosa* were grown in nutrient broth (0.3% beef extract and 0.5% peptone) to an early stationary phase (*i.e.* 18 h) at 37 °C. The culture was harvested by centrifugation at 10 000 rpm for 10 min and resuspended in K-media (2.4 g KCl, 3.1 g NaCl per litre) to give a final concentration of 10^7 CFU mL^{-1}. 25 mL of bacterial cells (10^7 CFU mL^{-1}) were incubated with 2 mg mL^{-1} of NSAgNP (containing 3.5 wt% Ag) and pristine nano-silica separately. Aliquots were taken out at different intervals and plated on the nutrient agar plates to grow bacteria at 37 °C for overnight. The number of viable cells was determined by the colony count method. The percentage killing efficiency (% kill) was measured as $[(N_{\text{nano-silica}} - N_{\text{NSAgNP}})/N_{\text{nano-silica}}] \times 100$, where $N_{\text{nano-silica}}$ and N_{NSAgNP} are the number of bacteria grown in the presence of nano-silica and NSAgNP, respectively.

Inhibition of biofilm formation on NSAgNP was assayed using *E. coli* as a model organism. 25 mL of *E. coli* (10^7 CFU mL^{-1}) culture was taken in different 100 mL Erlenmeyer flasks and 2 mg mL^{-1} of pristine nano-silica and NSAgNP (3.5 wt% Ag) were added separately followed by addition of 0.1% glucose. The flasks were then incubated in static condition at 37 °C for 24 h. After incubation the media were removed carefully and fresh 20 mL sterile nutrient broth was added to each flask. The media was removed and spiked with fresh sterile nutrient broth at alternate days. This was continued for 4 days. The growth of *E. coli* in the suspension was monitored spectrometrically by noting the absorbance value at 600 nm on each day. At the end of 48 and 96 h, both pristine nano-silica and NSAgNP were washed very carefully with sterile double distilled water to remove loosely attached cells from the surfaces. The biofilm formation was measured by crystal violet staining and LIVE/DEAD viability kit (Invitrogen, CA) (see ESI†).

The cell viability in the biofilm was tested and quantified by fluorescence microscopic and spectroscopic analyses, respectively. The biofilm was stained by LIVE/DEAD kit as described by the manufacturer. The nano-silica and NSAgNP were dispersed in double distilled water and the spectra were recorded on a fluorescence spectrometer (Varian Cary Eclipse). For blank, pristine nano-silica and NSAgNP were stained by LIVE/DEAD kit as above, and absorbance values were recorded. The relative spectra of the biofilms were acquired by subtracting the absorbance values of the respective blanks. The results are reported as average absorbance values of the triplicate measurements of the samples. The percentage anti-adhesion

property of NSAgNP was determined as $[(N_{\text{nano-silica}} - N_{\text{NSAgNP}})/N_{\text{nano-silica}}] \times 100$, where $N_{\text{nano-silica}}$ and N_{NSAgNP} are the number of viable cells present on nano-silica and NSAgNP, respectively.

Fluorescence microscopic images were recorded on a fluorescence microscope (Olympus BX-61) using an excitation filter of BP 460–495 nm and a band absorbance filter covering wavelengths below 505 nm. Live and dead cells were viewed in the same microscopic fields separately with different fluorescence filter sets. The cell viability was then assayed by counting green (live) and red (dead) cells. The biofilm structure on nano-silica and NSAgNP were monitored by scanning electron microscopic (SEM) images. Fixation of the biofilm was carried out following the protocol as described previously.[39] In brief, NSAgNP and nano-silica were thoroughly washed with phosphate buffer (50 mM, pH 7.2), and then fixed with 2.5% glutaraldehyde solution for 4 h followed by dehydration with graded ethanol series. The dried samples were then coated with gold and micrographs were recorded at random locations on a SEM instrument.

Stability and filtration test of NSAgNP using simulated wastewater

Simulated contaminated water relevant to the environmental conditions was prepared in 50 mM phosphate buffer (pH 7.0) by mixing dyes (equal amount of CR, EY, BPB, and BB) and *E. coli* to a final concentration of 50 mg L^{-1}, and 10^4 CFU mL^{-1}, respectively. To this solution, glucose (0.1%) and NaCl (0.1%) were also added and the resulting contaminated water was used as the feedwater for removal study to test the feasibility of NSAgNP under environmental conditions. The removal of dyes and *E. coli* from this contaminated water was studied using both NSAgNP and pristine nano-silica under identical conditions as described above at different time intervals. For stability experiments, aliquots were taken out at different time intervals and the concentrations of leached silver were measured with a flame atomic absorption spectrometer (Varian Spectra AA 55, USA) against a standard silver solution.

Results and discussion

Synthesis and characterization of NSAgNP

Synthesis of new functional nanomaterial with high adsorption, antimicrobial and antifouling properties has recently gained significant attention.[20,22,40] Inspired from natural biomineralization processes a two step process was followed, as illustrated in Scheme 1A, in order to fabricate AgNPs on a nano-silica support and simultaneously coating synthesized AgNPs with proteins. In the *in situ* synthesis process, silver nitrate solution was initially incubated with nano-silica powder, which caused rapid adsorption of positively charged Ag^+ ions on the electronegative surface and void of nano-silica through electrostatic interaction.[41] Large numbers of hydroxyl groups are present on the silica surface, which imposed a negative charge on the nano-silica material.[42] The adsorbed Ag^+ ions were then reduced by a protein extract of *R. oryzae*. The reduction of Ag^+ ions by the protein extract, without addition of any chemical reagent, led to a gradual change of the nano-silica color from white (Fig. 1A, left panel) to light brown and finally to deep brown (Fig. 1A, right panel) within 48 h. This indicated the formation of AgNPs on the nano-silica surface, which was referred as nano-silica silver nanomaterial (NSAgNP). The brown colored NSAgNP was separated from the solution by centrifugation, dried at 50 °C and finally dispersed in deionized water. The UV-vis spectra (Fig. 1B) of the dispersed solution exhibited an absorption maximum at 414 nm due to the surface plasmon resonance band (SPR) of the AgNPs.[37] However, silver nitrate solution treated with nano-silica only, without protein extract, remained colorless even after 96 h, and did not show any SPR band of AgNPs. This clearly demonstrated the microbial protein directed 'green synthesis' of AgNPs on the surface of nano-silica.

Transmission electron micrographs (TEM) clearly showed the synthesis of well dispersed AgNPs on the surface of nanoporous silica material (Fig. 1C). The particle size distribution determined from multiple TEM images demonstrated the formation of highly monodisperse spherical AgNPs (Fig. 1D) with an average size of 10 ± 2.5 nm. High resolution image (Fig. 1E) of a single AgNP showed the lattice distance of 0.23 nm (as marked in Fig. 1E), which was consistent with the Scherrer ring pattern (Fig. 1E, inset) observed in the selected area electron diffraction (SAED) of AgNPs. This was associated with the [111], [200], [222], and [311] atomic planes of the face centered cubic (fcc) lattice of nano-crystalline AgNPs.[37,43] In this process, the negatively charged protein bound with AgNPs surface served as both a reducing and stabilizing agent.[34,36] The as synthesized NSAgNP were stable over a period of four months without showing any aggregation of AgNPs as observed by the SPR band. It is also worth mentioning that the synthetic reactions were carried out at ambient temperature in the absence of any additional chemical agent and aqueous medium. The proposed *in situ* synthetic protocol therefore, provides a 'green' method for functional nanomaterial synthesis.

Energy-dispersive X-ray spectroscopic analysis (EDXA) of NSAgNP was carried out in the area profile mode, which depicted characteristic peaks for AgNPs at ~3.00 keV (Fig. 1F) in addition to the corresponding peaks of Si, C, N and O. The resulting Si and O peaks originated from supported nano-silica material, whereas C and N peaks demonstrated binding of proteins on the nanoparticle surface. In the control nano-silica (Fig. S1†), only peaks of Si, O and a small amount of C (perhaps from contamination) appeared. The quantitative elemental analysis demonstrated that NSAgNP contained 3.5 wt% Ag.

The speciation and chemical composition of NSAgNP was studied through X-ray photoelectron spectroscopic (XPS) technique. Fig. 2A presents wide-scan XPS elemental survey spectra of nano-silica and NSAgNP. Presence of C 1s, O 1s, and Si 2p peaks were observed in nano-silica, while additional peaks of N 1s, and Ag 3d appeared in NSAgNP as expected. The high resolution spectra of Si 2p (Fig. 2B) appeared at 102.1 eV both in nano-silica and NSAgNP, which corresponded to SiO_2. The O 1s spectrum (Fig. 2C) in nano-silica deconvoluted into two peaks centered at 530.1 and 531.6 eV, which could be ascribed to Si–O in SiO_2 (nano-silica) and surface O–H groups, respectively.[44] The

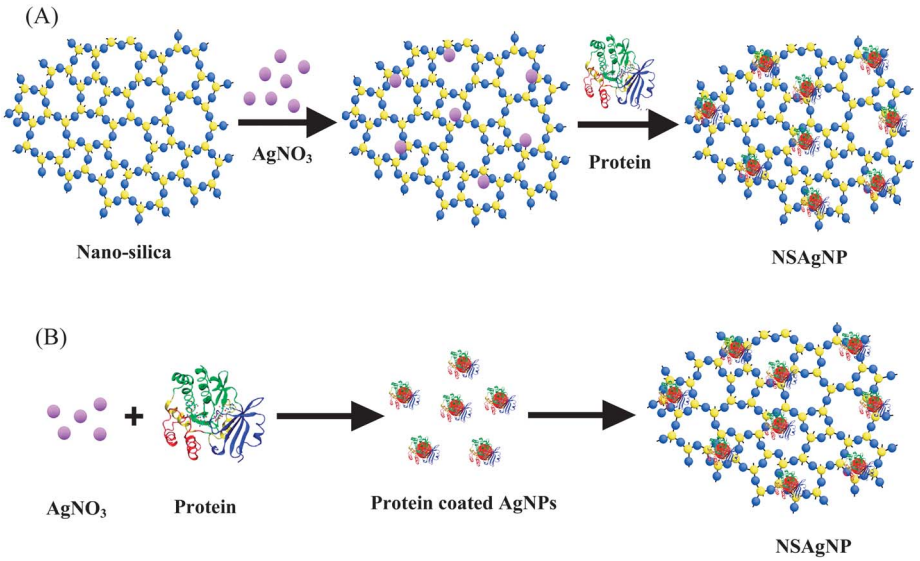

Scheme 1 Schematic illustration of the *in situ* synthesis (A) of AgNPs on nano-silica support (NSAgNP) by protein extract, (B) immobilization of protein coated AgNPs on nano-silica support by the 'post-deposition' route.

peak intensity of O–H species was significantly higher than that of Si–O, which indicated that hydroxyl groups were present on the nano-silica surface in large amounts. The O 1s BE (binding energy) appeared at a lower value (531.3 eV) in NSAgNP compared to the nano-silica. Moreover, the intensity of the O–H peak was lowered after AgNP formation. This demonstrated binding of AgNPs with SiO_2 through electrostatic interaction of O–H groups. The high resolution core level spectra of Ag 3d (Fig. 2D) in NSAgNP was composed of doublet peaks at 367.6 and 373.8 eV, and assigned to $3d_{5/2}$ and $3d_{3/2}$ peaks of Ag^0, respectively. The gap of 6.2 eV between the two states was also indicative of metallic Ag^0,[45] and corroborated with the EDXA analysis. However, the Ag $3d_{5/2}$ BE appeared at a lower value (367.6 eV) compared to the Ag^0 (BE of Ag $3d_{5/2}$ for Ag^0 is about

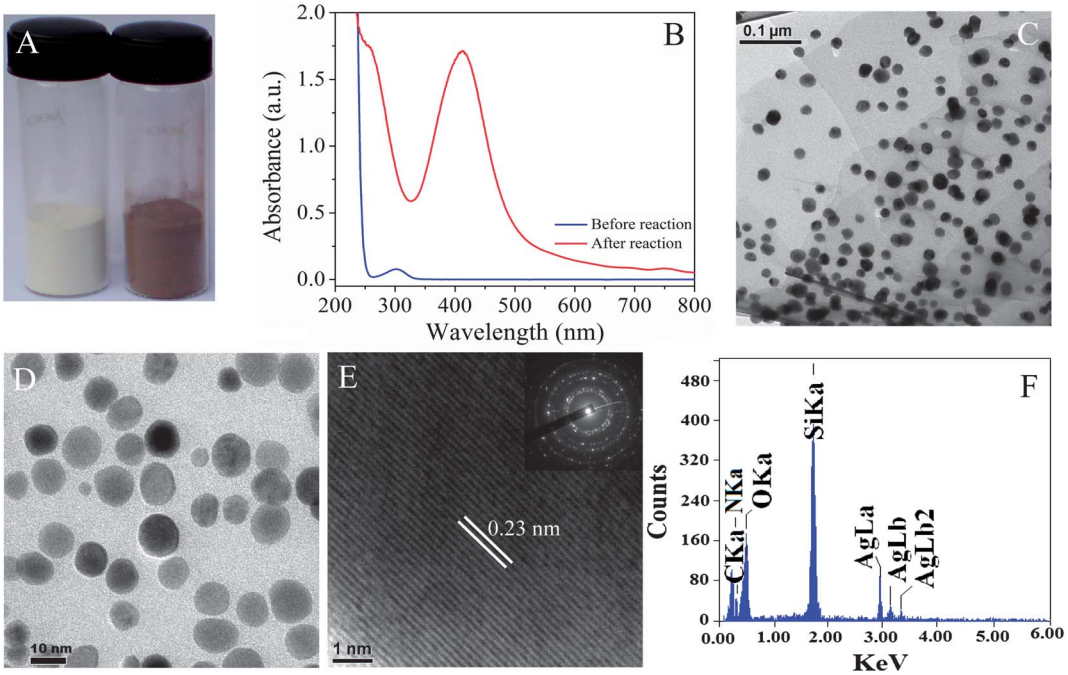

Fig. 1 Images (A) of nano-silica (left panel), and NSAgNP (right panel); UV-vis spectra (B) of the dispersed solution of nano-silica before and after reaction with $AgNO_3$ solution in presence of protein (NSAgNP); TEM micrograph (C) demonstrating formation of AgNPs on the surface of nano-silica; the high resolution image (D) shows the formation of ~10 nm diameter spherical AgNPs; lattice space (E) and selected area diffraction pattern (inset) of AgNPs; EDXA spectrum (F) of NSAgNP recorded in spot profile mode.

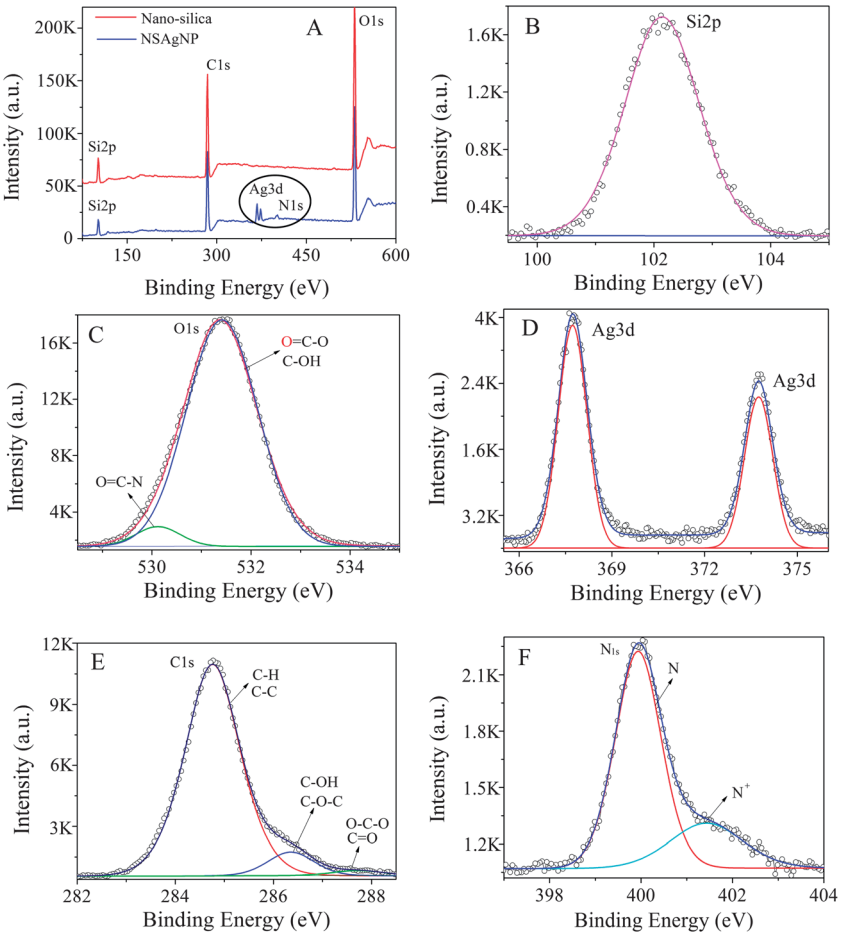

Fig. 2 XPS survey spectra (A) of nano-silica and NSAgNP; high resolution core level spectra of Si 2p (B), O 1s (C), Ag 3d (D), C 1s (E), and N 1s (F), respectively.

368.2 eV), which further demonstrated binding of AgNPs with SiO_2.[46] The analysis of the core-level spectra of C 1s, and N 1s clearly demonstrated the presence of the protein molecules in NSAgNP.[32,36,47] The C 1s spectrum could be resolved into four components at BE of 282.4, 285, 286.6, and 288.4 eV (Fig. 2E) assigning them to the four different chemical components (C–C, C=C, C–N, C–OH, C=O, *etc.*) of protein molecules. The N 1s peak at 399.7 and 401.4 eV (Fig. 2F) could be assigned to the N–C=O and $-NH_2$ bonding of protein molecules. This result clearly indicated that proteins were present in NSAgNP. Silver has high redox potential [$E^0_H(Ag^+/Ag^0) = 0.8$ V], which led to the "grabbing" of electron from proteins, resulting in reduction of Ag^+ to Ag^0. Previously we have demonstrated that the carboxyl and amine groups of proteins are responsible for their reduction and the subsequent formation of metal nanoparticles.[32,36,37] The surface attached proteins therefore, served as reducing and stabilizing agents in the bioinspired synthesis of NSAgNP and formed an inorganic–organic hybrid nanomaterial.

In an alternative method, protein coated AgNPs were immobilized on a nano-silica surface by a post deposition method.[48,49] In brief, the protein coated AgNPs were initially synthesized in a similar manner following reaction of $AgNO_3$ with protein extract, which were then incubated with nano-silica (Scheme 1B) leading to the fabrication of protein functionalized AgNPs on the nano-silica surface. Interestingly, similar results were obtained (ESI Fig. S2†) to the *in situ* reduction process (Scheme 1A), and thus the protein served both as reducing as well as stabilizing agent for AgNPs. The experimental results thus confirmed protein mediated bio-inspired synthesis of the NSAgNP hybrid material.

Adsorption of dyes by NSAgNP

The adsorptive removals of various anionic and cationic dyes like CR, EY, BB, BPH and mixed cocktail dyes (CD) were studied using the as-synthesized NSAgNP material. It was found that almost 99% of the dyes were removed by NSAgNP at an initial concentration of 50 mg L^{-1}. Fig. 3A shows color photographs of the dye solution before and after treatment with NSAgNP; and without exception, the dye solution became colorless within 30 min of treatment. This result clearly demonstrated the versatility of NSAgNP in adsorptive removal of all these dyes.

The process was further optimized through varying the solution pH, contact time and dye concentration. The effect of pH on adsorption of these dyes was studied at different pH conditions since it influences not only the charge density of an adsorbent but also the mobility of the adsorbate.[39,50] It was found that CR, EY, and BB more effectively adsorbed (Fig. 3B) at

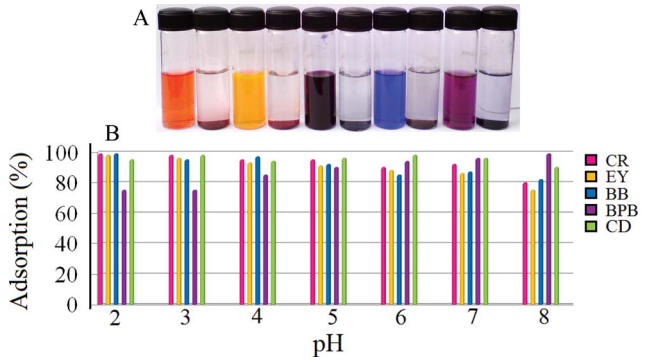

Fig. 3 Photographs (A) of a series of dyes solutions before and after treatment with NSAgNP; percentage removal of dyes (B) at different pH values (2.0–8.0). Bottles from left to right: CR, EY, BB, BPH and mixed cocktail dye (CD). Dye concentration is 50 mg L^{-1}.

low pH conditions (2.0–4.0). Almost 99% of the initial dyes were removed at these pH values and their adsorption capacities decreased moderately (~20%) with further increase in pH values. CR, EY, and BB are anionic dyes and, therefore, favourably adsorbed through electrostatic interaction by binding with positively charged adsorbent at low pH values.[7,39] Besides, physical adsorption between the pore of nano-silica and π–π interaction with sp^2 bonded Si–O also took place and through limited adsorption of dyes at higher pH values.[7,9,51,52] On the other hand, BPH is a cationic dye and hence the reverse was observed, as expected. In this case more dye was adsorbed at high pH values and about 99% of dye was adsorbed at above pH value 8.0. This result therefore, suggested that acid–base interactions were involved in the dye adsorption process. It is worthwhile to mention that similar quantities of dyes were adsorbed by nano-silica under identical conditions, which indicated that AgNPs immobilization did not affect the adsorption capacity of nano-silica.

The wastewater discharged from the textile and leather industries often contains multicomponent dyes. To test the feasibility of NSAgNP in the removal of dyes in multicomponent system, a cocktail dye (CD) was prepared (see the Experimental section), which mimics the polluted water, and adsorptive removal on this system was studied. This mixed cocktail dye was then adsorbed by NSAgNP conditioned at different pH values. Surprisingly, it was observed that in all pH ranges (2.0–9.0), the corresponding adsorption values could hardly be discriminated and more than 98% dye was adsorbed at an initial dye concentration of 50 mg L^{-1}. This clearly showed that adsorption behavior in the multicomponent system was quite different to that of single component system. However, the interaction of mixed dyes with NSAgNP occurred in a more complex way. The exact binding mechanism is not known at this moment and called for further study in the future.

The effect of contact time on adsorption of the mixed cocktail dye was also studied at three different pH values (4.2, 6.8, and 9.1). Fig. 4A shows images of dye solutions at various time intervals which became colorless within 30 min. A rapid decrease in dye concentration (Fig. 4B) was observed within the first 5 min and reached an equilibrium at around 20 min; thereafter it decreased slowly. The adsorption capacities of this dye were 24.69, 23.94, and 23.75 mg g^{-1} at pH values of 4.2, 6.8 and 9.1, respectively, which demonstrated that both adsorption capacity and rate remain unaltered within this broad pH range. The multiplex adsorbability of NSAgNP under a wide pH range thus suggested that this hybrid nanomaterial is extremely useful in realistic polluted water treatment. The rapid adsorption of the mixed dyes was attributed to the high surface area and presence of large numbers of hydroxyl groups on NSAgNP, which favored the surface binding of various types of dyes on NSAgNP through electrostatic and π–π interaction, though diffusion between the particles also took place to a certain degree. The faster kinetics also ensured high efficiency and thus had a significant practical importance in large scale applications. The kinetics data were further analyzed with different rate kinetics models like the pseudo-first (ESI, Fig. S3A†), second order (ESI, Fig. S3B†) and intra-particle diffusion models (ESI, Fig. S4†) to determine the rate controlling and mass transfer mechanism (see ESI† for details).[7,53,54] The experimental results showed that rate kinetics followed perfectly pseudo-second-order rate model with very high correlation coefficients of 0.999 (Table S1†). It has also been suggested that the surface adsorption played a dominant role, though certain amount of diffusion into the pore of the adsorbent also took place.

The maximum adsorption capacity (Q_{max}, mg g^{-1}) was obtained from an equilibrium adsorption isotherm study as shown in Fig. 4C. The adsorption capacity increased with dye concentration and finally reached equilibrium imparting a maximum dye adsorption capacity of NSAgNP was 547.5 ± 35.2 mg g^{-1}, which is much higher than the commercial activated carbon. Under identical conditions, activated carbon had six times less adsorption capacity than NSAgNP and adsorbed only 85.8 ± 7.4 mg g^{-1} dye (ESI, Fig. S5†). The maximum adsorption capacity of NSAgNP is also much higher than those reported in the literature (ESI, Table S2†). For example, a reduced graphene oxide–Fe_3O_4 hybrid adsorbed 44.4 mg g^{-1} rhodamine B,[9] cross-linked PEI/PVA nanofibrous mats adsorbed 209.63 mg g^{-1} methyl blue,[53] while carboxyl functionalized superparamagnetic mesoporous silica microspheres adsorbed 101.9 and 109.6 mg g^{-1} methylene blue and acridine orange, respectively.[55] The very high adsorption capacity and efficiency of NSAgNP towards multiplexed dye solution compared to the other adsorbents might be attributed to the high surface area and surface active groups which provided electrostatic binding of dye molecules with a large number of surface hydroxyl groups, π–π interaction with sp^2 bonded Si–O, and physisorption between the pore of the adsorbent. Carboxyl and amine groups of bound proteins on NSAgNP might also participate in dye adsorption and contribute to high adsorption capacity of NSAgNP.

The present adsorption system typically followed type I isotherm behavior, according to the IUPAC classification, and obeyed the Langmuir isotherm model (Fig. 4C, inset) among other two parameter isotherm models (ESI Fig. S6 and Table S3†) namely Freundlich, Dubinin–Radushkevitch and Temkin.[7,56,57] This indicated that chemical force played a dominant role, while physical interaction also participated to some extent in the adsorption of multiplex dyes on NSAgNP.

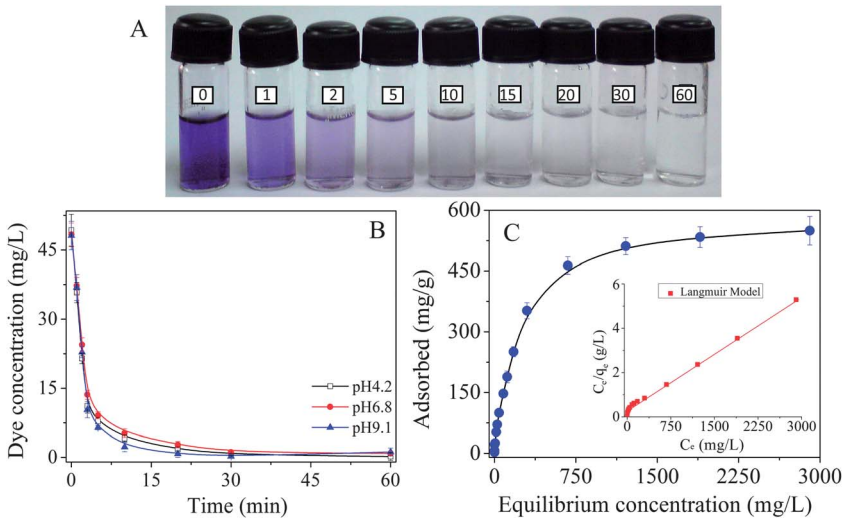

Fig. 4 Photographs (A) of mixed cocktail dye solution treated with NSAgNP at different time intervals; kinetics (B) and adsorption isotherm (C) of cocktail dye on NSAgNP. Inset in (C) demonstrates fitting of the isotherm data with a Langmuir model.

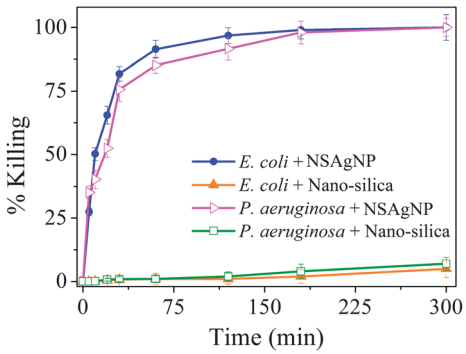

Fig. 5 Killing percentage of *E. coli* and *P. aeruginosa* by nano-silica and NSAgNP.

Recovery and re-use of NSAgNP material

Recovery and re-use of NSAgNP was further carried out through desorption of dye from loaded NSAgNP for safe disposal of the adsorbent and to minimize solid waste generation. Among all tested mineral acids, bases and organic solvents, acetone removed 86% of the adsorbed dye (ESI Table S4†). Mineral acids and bases were mostly ineffective in this respect and desorbed only around 20–30% of the adsorbed dye. This demonstrated that π–π interaction, between the sp^2 group of Si–O on SiO_2 and the phenyl group of dyes, is the main dye binding mechanism on NSAgNP. The regenerated NSAgNP retained around 78 ± 2% of its original adsorption capacity. A decrease in the active surface area of the sp^2 group due to contamination by dye residues during the regeneration process might be responsible for the reduction of adsorption capacity. Geng *et al.*[9] also observed a similar phenomena for the adsorption of dyes on a reduced graphene oxide–Fe_3O_4 nanoparticles hybrid. The regeneration efficiency thus makes the NSAgNP potentially suitable for high-efficiency and low-cost water pollution treatment.

Antibacterial effect of NSAgNP material on planktonic cells and biofilm formation inhibition

The bactericidal activity of NSAgNP was investigated against two Gram-negative bacteria, namely *E. coli* and *P. aeruginosa*, because a large population of these pathogenic bacteria are always present in water-bodies and cause waterborne diseases. The effect of NSAgNP on these bacteria was carried out by the spread plate method. The killing kinetics showed a typical time dependent antibacterial activity (Fig. 5). More than 80% of bacteria were killed within an hour after interaction with NSAgNP and very few bacterial colonies were observed on nutrient agar plates after 3 h (Fig. 6B and D) interaction. In contrast, the control experiment with the pristine nano-silica under otherwise identical conditions showed a dense growth of *E. coli* (Fig. 6A) and *P. aeruginosa* (Fig. 6C) colonies and, thus, highlighted excellent antimicrobial activity of NSAgNP against these organisms. The killing efficiency increased with increase in exposure time and 3 h was sufficient for killing of these pathogens. The viability of the treated bacterial cells was further investigated by a LIVE/DEAD assay. Fig. 6E and G showed that nano-silica treated *E. coli* and *P. aeruginosa* cells were stained green (SYTO 9 staining indicates live cells), whereas NSAgNP treated cells (Fig. 6F and H) mostly stained with the red color (propidium iodide staining indicates dead cells). The two stains SYTO 9 and propidium iodide (PI) differ in their permeability to the bacterial cells. SYTO 9 stains both live and dead cells; however PI is permeable only through the damaged cell membrane and thus stains dead cells in particular. Thus, the cell membrane disruption by NSAgNP killed the bacterial cell, which corroborates with earlier reports.[58–60] A similar antibacterial activity was also observed with two months old NSAgNP, though inhibition of antibacterial activity was reported for 5-days-old bare AgNPs due to oxidation and/or aggregation of AgNPs in air.[61,62] The higher stability of AgNPs in NSAgNP might be responsible for both the high and long-term antibacterial

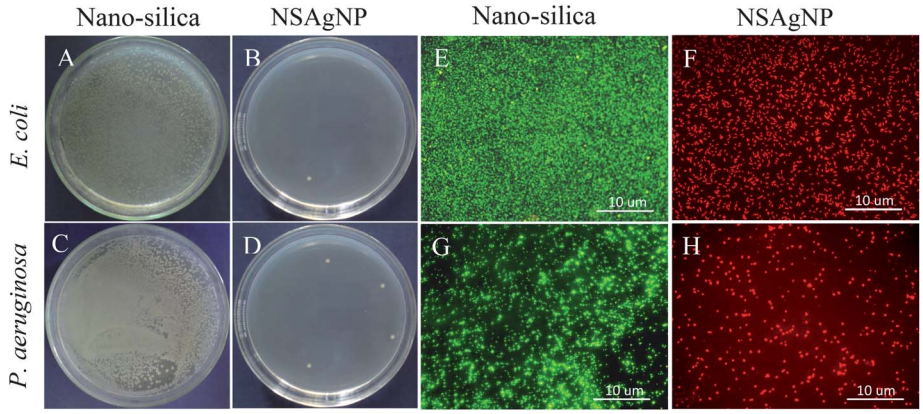

Fig. 6 Petri dishes with NB-agar inoculated with *E. coli* (A and B) and *P. aeruginosa* (C and D) incubated in presence of 2.0 mg mL^{-1} of nano-silica (A and C) and NSAgNP (B and D), respectively for 24 h at 37 °C; viability of *E. coli* (E and F), and *P. aeruginosa* (G and H) cells following treatment with nano-silica (E and G) and NSAgNP (F and H), respectively for 2 h. Cells were stained with SYTO 9 and propidium iodide and micrographs were recorded on a fluorescence microscope (Olympus BX-61) using an excitation filter of BP 460–495 nm and a band absorbance filter covering wavelengths below 505 nm.

activity of NSAgNP compared to that of AgNPs. The immobilization of protein-coated AgNPs thus significantly improved the antibacterial property of NSAgNP.

The bactericidal activity of NSAgNP was further investigated for long term activity specially in biofilm formation. Although AgNPs demonstrated short term antibacterial activity, the instability of AgNPs due to leaching of Ag^+ ions and aggregation of AgNPs through oxidation prevents its application for long term application. Taurozzi *et al.*[63] reported that a silver-embedded polysulfone membrane was unable to prevent biofilm formation of *E. coli*. The biofilm formation in the treatment plant often reduces its efficiency and also created significant health issues. To investigate the antifouling and antibacterial properties of NSAgNP on inhibition of biofilm formation, *E. coli* was allowed to grow over a period of 96 h. Bacterial growths in the suspension as well as on the material surfaces were adopted to measure biofilm formation.[64] The cell growth in the suspension was visualized (Fig. 7A-I) in the nano-silica treated *E. coli* following the media change, however, no visible cell growth was evident in the NSAgNP treated culture (Fig. 7A-II). Bacterial growth was further monitored by turbidity (OD_{600}) on consecutive 48 and 96 h (see the Experimental section). The pristine nano-silica treated culture led to full bacterial growth, which increased with time (Fig. 7B) and lead to the formation of a biofilm. The biofilm formation on the pristine nano-silica and NSAgNP was confirmed by crystal violet staining. This result showed that AgNPs immobilization significantly improved the biofilm inhibition properties (Fig. 7B) of NSAgNP and prevented further growth of bacteria. On the other hand, pristine nano-silica was unable to inhibit the bacterial growth. The attached cells grew with time and lead to thick biofilm formation. Zeta potential measurement of NSAgNP showed a positive zeta value (0.75 mV) of the NSAgNP suspension. Therefore, it appears that the mechanism of the antibacterial activity of NSAgNP may involve electrostatic interaction with negatively charged bacterial cell membranes or membrane proteins. The bacterial cell surface possesses a net negative charge at pH values >5.0 due to the presence of ionized phosphoryl and carboxylate groups on cell membrane proteins and carbohydrate molecules.[65] The strong interaction of NSAgNP with the cell membrane results in physical damage followed by cell death. Huang *et al.*[65] also proposed that the capture and removal of several Gram positive and Gram negative bacterial species was driven by electrostatic interaction of amine functionalized magnetic nanoparticles.

The antifouling or anti-adhesion property of NSAgNP and viability of the attached cells was confirmed and quantified by fluorescence spectroscopic analysis after 96 h of incubation. Fig. 7C shows fluorescence spectroscopic measurement of nano-silica and NSAgNP treated cells following staining with SYTO 9 and PI. The percentage of live and dead cells on nano-silica and NSAgNP were calculated from the spectroscopic data (Table 1), which demonstrated that ~95% cells were alive on nano-silica, as it stained by SYTO 9; but a much lesser amount of dead cells were present on NSAgNP. To visualize the live and dead cells on nano-silica and NSAgNP the fluorescence microscopic images were recorded, which showed that a thick and complex biofilm of *E. coli* was formed on nano-silica, where most of the cells were live (Fig. 7D). On the other hand, NSAgNP had approximately 100 times less cells, and just a few dead cells (PI stained red cells) were remained on NSAgNP (Fig. 7E). These results undoubtedly established the antibacterial and antifouling properties of NSAgNP.

SEM analysis further demonstrated the bacterial growth and structure of the biofilms on the surface. Healthy rod shaped *E. coli* and a biofilm network structure was evident on the nano-silica surface (ESI Fig. S7A and B†). The cells were trapped or adhered tightly on the nano-silica surface and grew further to form a biofilm network. In contrast, a biofilm was not observed on the entire surface of NSAgNP; only a few scattered dead cells were spotted (marked by a circle in the ESI Fig. S7C†), indicating that *E. coli* could not survive at all on the NSAgNP. The high magnification SEM image (ESI Fig. S7D†) showed that the cell became distorted and damaged, which was probably due to direct interaction of the cell and NSAgNP. Additionally, the stressed cells elongated without apparent cellular division; the cell walls were roughed, cracked and ruptured. In stress

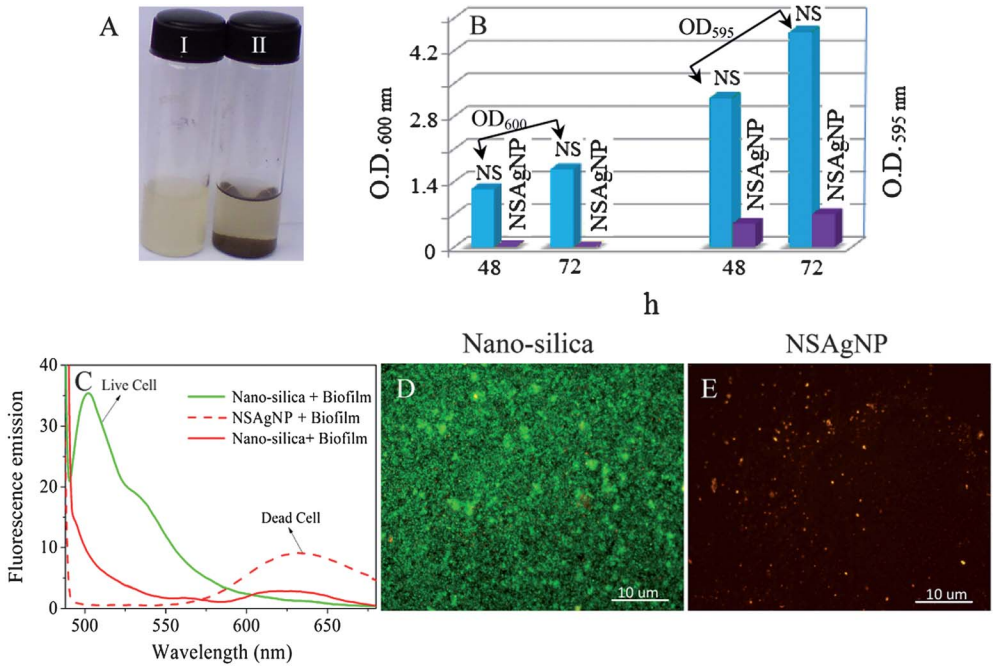

Fig. 7 Photographs (A) of bacterial growth in presence of nano-silica (I) and NSAgNP (II); bacterial growth *vs.* biofilm formation (B) in nano-silica and NSAgNPs; fluorescence spectra (C) of dispersed solution of nano-silica and NSAgNP after incubation with *E. coli* for 72 h. Cell viability test of biofilms formation of *E. coli* on nano-silica (D) and NSAgNP (E) following staining with SYTO 9 and propidium iodide. Micrographs were recorded on a fluorescence microscope (Olympus BX-61) using an excitation filter of BP 460–495 nm and a band absorbance filter covering wavelengths below 505 nm.

Table 1 The anti-bacterial and anti-adhesion properties of NSAgNP compared to nano-silica

Material	% Antibacterial[a]	% Anti-adhesion[b]
NSAgNP	99.9	99.5%

[a] Antibacterial activity $= [(N_{\text{nano-silica}} - N_{\text{NSAgNP}})/N_{\text{nano-silica}}] \times 100$, where $N_{\text{nano-silica}}$ and N_{NSAgNP} are number of bacteria grown in the presence of nano-silica and NSAgNP, respectively. [b] Anti-adhesion $[(N_{\text{nano-silica}} - N_{\text{NSAgNP}})/N_{\text{nano-silica}}] \times 100$, where $N_{\text{nano-silica}}$ and N_{NSAgNP} are the number of viable cell present on nano-silica and NSAgNP, respectively.

conditions the filamentation of *E. coli* was reported.[66] Lesions and holes were also noticed in the cell (as indicated by arrows in the Fig. S7D†) after contact with the NSAgNP. A similar observation was also reported by Ahmed *et al.*,[17] where *E. coli* and *B. subtilis* were treated with PVK-SWNT nanocomposites. This study therefore, demonstrated that immobilization of AgNPs on nano-silica significantly improved the antibacterial and anti-fouling properties of NSAgNP, which in turn prevented biofilm formation for prolonged times. The mechanism of biofilm formation was reported to occur in three stages: (i) initial adsorption; (ii) irrereversible adhesion to the surface; and (iii) colonization.[20] Considering these three stages, it can be inferred that due to the strong antibacterial activity of NSAgNP, the initial attachment of bacteria on NSAgNP was strongly inhibited and thus prevented biofilm formation. A similar antifouling property of the Ag/MWNTs/PAN composite has very recently been reported by Gunawan *et al.*[22]

Treatment of simulated contaminated water with NSAgNP material

The long-term stability, antifouling property and leaching of silver from NSAgNP were assayed under simulated environmental conditions. Simulated contaminated water was prepared by mixing dyes, *E. coli*, glucose, NaCl and treating with NSAgNP for 4 days. Glucose in the medium provided a nutritious environment to minimize bacterial death because of the high concentration of bacterial cells often present in wastewater. In addition, chloride ions in water are reported to reduce the antibacterial activity of AgNPs by formation of an AgCl layer.[67,68] The results (ESI, Table S5†) showed that in the presence of glucose and NaCl did not affect the performance of NSAgNP and with time both the concentration of dye and *E. coli* reduced significantly. The dye was not detected in the solution within 30 min; the initial *E. coli* concentration of 85×10^3 reduced dramatically to 102 ± 11 within this time period, and was not detected after 3 h treatment. No further growth of *E. coli* was observed even after 4 days. The control experiment using pristine nano-silica was able to reduce the dye concentration but was unable to inhibit the bacterial population and final biofilm formation. The antibacterial activities and stability of AgNPs were reported to influenced by: different ligands such as O_2, Cl^-, PO_4^-; organic molecules present in the aqueous system; and the nature of the supporting matrix.[67–69] These interact with AgNPs and change both their composition and structure. Other studies also showed that Ag^+ ions are leached out from AgNPs in an aquatic environment and reduce the bioavailability of AgNPs.[42,70] Additionally, the

release of Ag^+ ions could have potential risks for environmental contamination and the development of bacterial resistance.

The leaching of Ag^+ ions from NSAgNP in the treated water was studied by AAS analysis at different time intervals, however, no apparent leaching of Ag^+ was detected. The NSAgNP thus exhibited enough stability and antibacterial activity to prevent biofilm formation in environmental conditions. The protein coating on AgNPs inhibited the diffusion of ions or ligands at the interface of AgNPs and thus prevented the leaching of Ag^+ ions. Another possibility is that nano-silica adsorbed the ligands and protected AgNPs from these ligands, resulting in additional stability of NSAgNP. Overall these results demonstrated the importance of nano-silica and protein coating for stability and reactivity of NSAgNP. Thus, the proposed NSAgNP was very resistant to all these ligands and the antibacterial activity including stability remained unaffected in environmental conditions. Our findings suggest that the high surface area and surface active sites of NSAgNP contribute to a high adsorption capacity and efficient removal of multiplexed dye from water bodies. The antifouling property of NSAgNP further prevents biofilm formation on the surface and, therefore, can be used for water treatment for prolonged times. In addition, the reusability of NSAgNP will reduce the operational cost of water treatment technology. We therefore, strongly believe that the efficient dye adsorption, antifouling and reusability properties of NSAgNP have significant practical importance in the development of a nanotechnology based approach for the treatment of wastewater.

Conclusions

Bioinspired synthesis of AgNPs functionalized nano-silica (NSAgNP) has been developed as antifouling nanomaterial for sustainable water purification. AgNPs of 10 ± 2.5 nm size were synthesized on the surface of nano-silica through protein mediated reduction of bound silver ions on nanoporous silica. The proteins served both as a reducing and a protecting agent for AgNPs and prevented oxidation of AgNPs under environmental conditions. The synthesized nanomaterial exhibited very high adsorption capacities for various dyes even in multicomponent system and presence of other interfering ligands, which demonstrated strikingly good multiplex adsorbability. More importantly, the adsorption performance of the nanomaterial showed satisfactory tolerance to variations in pH value, dye concentration, coexistence of multiple dyes, and other ligands. Chemical interaction including π–π interaction, and pore diffusion contributed simultaneously to the adsorption phenomenon. Furthermore, AgNP fabrication significantly enhanced the antimicrobial and antifouling properties of the nano-composite and thus prevented biofilm formation under laboratory as well as simulated environmental conditions. The long term antibacterial, antifouling and high dye adsorption properties of this functional nanomaterial are exceptionally promising for the development of high-efficiency and low cost water purification technologies.

Acknowledgements

S. K. Das acknowledges Department of Biotechnology (DBT), Government of India for research support under the Rapid Grant for Young Investigators (RGYI). The authors also gratefully acknowledge the Council of Scientific and Industrial Research (CSIR), Government of India for financial assistance under the STRAIT programme.

References

1 P. Raskin, *et al.*, *Water Futures: Assessment of Long-Range Patterns and Problems, Comprehensive Assessment of the Freshwater Resources of the World*, Stockholm Environment Institute, Stockholm, 1997, p. 23.
2 Y. Wong and J. Yu, *Water Res.*, 1999, **33**, 3512–3520.
3 R. O. Alves de Lima, A. P. Bazo, D. M. Salvadori, C. M. Rech, D. de Palma Oliveira and G. de Aragão Umbuzeiro, *Mutat. Res., Genet. Toxicol. Environ. Mutagen.*, 2007, **626**, 53–60.
4 R. F. Service, *Science*, 2006, **313**, 1088–1090.
5 G. Mezohegyi, F. P. van der Zee, J. Font, A. Fortuny and A. Fabregat, *J. Environ. Manage.*, 2012, **102**, 148–164.
6 S. Sekar, M. Surianarayanan, V. Ranganathan, D. R. MacFarlane and A. B. Mandal, *Environ. Sci. Technol.*, 2012, **46**, 4902–4908.
7 S. K. Das, I. Shome and A. K. Guha, *Sep. Sci. Technol.*, 2012, **47**, 1913–1925.
8 C.-Y. Cao, J. Qu, W.-S. Yan, J.-F. Zhu, Z.-Y. Wu and W.-G. Song, *Langmuir*, 2012, **28**, 4573–4579.
9 Z. Geng, Y. Lin, X. Yu, Q. Shen, L. Ma, Z. Li, N. Pan and X. Wang, *J. Mater. Chem.*, 2012, **22**, 3527–3535.
10 N. Wu, H. Wei and L. Zhang, *Environ. Sci. Technol.*, 2012, **46**, 419–425.
11 X. Fu, X. Chen, J. Wang and J. Liu, *Microporous Mesoporous Mater.*, 2011, **139**, 8–15.
12 L. Ai, H. Yue and J. Jiang, *Nanoscale*, 2012, **4**, 5401–5408.
13 Y. Wang, D. Chen, Y. Wang, F. Huang, Q. Hu and Z. Lin, *Nanoscale*, 2012, **4**, 3665–3668.
14 R. Mallampati and S. Valiyaveettil, *Nanoscale*, 2013, **5**, 3395, DOI: 10.1039/c3nr34221b.
15 V. K. K. Upadhyayula and V. Gadhamshetty, *Biotechnol. Adv.*, 2010, **28**, 802–816.
16 G. O'Toole, H. B. Kaplan and R. Kolter, *Annu. Rev. Microbiol.*, 2000, **54**, 49–79.
17 F. Ahmed, C. M. Santos, R. A. M. V. Vergara, M. C. R. Tria, R. Advincula and D. F. Rodrigues, *Environ. Sci. Technol.*, 2012, **46**, 1804–1810.
18 A. Shukla, K. E. Fleming, H. F. Chuang, T. M. Chau, C. R. Loose, G. N. Stephanopoulos and P. T. Hammond, *Biomaterials*, 2010, **31**, 2348–2357.
19 X. Qi, G. Poernomo, K. Wang, Y. Chen, M. B. Chan-Park, R. Xu and M. W. Chang, *Nanoscale*, 2011, **3**, 1874–1880.
20 S. Kittler, C. Greulich, J. Diendorf, M. Köller and M. Epple, *Chem. Mater.*, 2010, **22**, 4548–4554.
21 G. M. Nisola, J. S. Park, A. B. Beltran and W.-J. Chung, *RSC Adv.*, 2012, **2**, 2439–2448.

22 P. Gunawan, C. Guan, X. Song, Q. Zhang, S. S. J. Leong, C. Tang, Y. Chen, M. B. Chan-Park, M. W. Chang, K. Wang and R. Xu, *ACS Nano*, 2011, **5**, 10033–10040.
23 M. Sureshkumar, D. Y. Siswanto and C. K. Lee, *J. Mater. Chem.*, 2010, **20**, 6948–6955.
24 U.S. EPA, Silver: Reregistration Eligibility Decision Fact Sheet. Prepared by the Office of Prevention, Pesticides And Toxic Substances, Environmental Protection Agency, Washington, DC, EPA-738-F-93–005, 1993.
25 J. Hagen, *Industrial Catalysis: A Practical Approach*, Wiley-VCH, Weinheim, 2006, pp. 223–237.
26 R. M. Rioux, H. Song, M. Grass, S. Habas, K. Niesz, J. D. Hoefelmeyer, P. Yang and G. A. Somorjai, *Top. Catal.*, 2006, **39**, 167–174.
27 Y. Xia, Y. Xiong, B. Lim and S. E. Skrabalak, *Angew. Chem., Int. Ed.*, 2009, **48**, 60–103.
28 C. Burda, X. Chen, R. Narayanan and M. A. El-Sayed, *Chem. Rev.*, 2005, **105**, 1025–1102.
29 R. Kumar and H. Münstedt, *Biomaterials*, 2005, **26**, 2081–2088.
30 X.-H. Li, X. Wang and M. Antonietti, *Chem. Sci.*, 2012, **3**, 2170–2174.
31 X. Gao and H. Matsui, *Adv. Mater.*, 2005, **17**, 2037–2050.
32 S. K. Das, C. Dickinson, F. Lafir, D. F. Brougham and E. Marsili, *Green Chem.*, 2012, **14**, 1322–1334.
33 F. Reith, L. Fairbrother, G. Nolze, O. Wilhelm, P. L. Clode, A. Gregg, J. E. Parsons, S. A. Wakelin, A. Pring, R. Hough, G. Southam and J. Brugger, *Geology*, 2010, **38**, 843–846.
34 S. K. Das, A. R. Das and A. K. Guha, *Small*, 2010, **6**, 1012–1021.
35 J. A. Dahl, B. L. S. Maddux and J. E. Hutchison, *Chem. Rev.*, 2007, **107**, 2228–2269.
36 S. K. Das, J. Liang, M. Schmidt, F. Laffir and E. Marsili, *ACS Nano*, 2012, **6**, 6165–6173.
37 S. K. Das, M. M. R. Khan, A. K. Guha, A. R. Das and A. B. Mandal, *Bioresour. Technol.*, 2012, **124**, 495–499.
38 R. Ramanathan, M. R. Field, A. P. O'Mullane, P. M. Smooker, S. K. Bhargav and V. Bansal, *Nanoscale*, 2013, **5**, 2300–2306.
39 S. K. Das, A. R. Das and A. K. Guha, *Langmuir*, 2009, **25**, 360–366.
40 F. Natalio, R. André, A. F. Hartog, B. Stoll, K. P. Jochum, R. Wever and W. Tremel, *Nat. Nanotechnol.*, 2012, **7**, 530–535.
41 D. Lee, Z. Gemici, M. F. Rubner and R. E. Cohen, *Langmuir*, 2007, **23**, 8833–8837.
42 J. Song, H. Song, H. Kong, J.-Y. Hong and J. Jang, *J. Mater. Chem.*, 2011, **21**, 19317–19323.
43 R. D. Glover, J. M. Miller and J. E. Hutchison, *ACS Nano*, 2011, **5**, 8950–8957.
44 C.-Y. Cao, J. Qu, W.-S. Yan, J.-F. Zhu, Z.-Y. Wu and W.-G. Song, *Langmuir*, 2012, **28**, 4573–4579.
45 H. Zhang, C. Liang, J. Liu, Z. Tian, G. Wang and W. Cai, *Langmuir*, 2012, **28**, 3938–3944.
46 J. F. Moulder, W. F. Stickle, P. E. Sobol and K. D. Bomben, *Handbook of X-Ray Photoelectronspectroscopy: A Reference Book of Standard Spectra for Identification and Interpretation of XPS Data*, Physical Electronics, Reissue edition, Physical Electronics, USA 18725, Lakedrive East, Chanhassen, MN 55317, 1995.
47 S. K. Das, M. Mukherjee and A. K. Guha, *Langmuir*, 2008, **24**, 8643–8650.
48 S. L. Christensen, A. Chatt and P. Zhang, *Langmuir*, 2012, **28**, 2979–2985.
49 H. Li, L. Han, J. Cooper-White and I. I. Kim, *Green Chem.*, 2012, **14**, 586–591.
50 S. K. Das and A. K. Guha, *J. Hazard. Mater.*, 2009, **167**, 685–691.
51 S. Chatterjeea, S. K. Das, R. Chakravarty, A. Chakrabarti, S. Ghosh and A. K. Guha, *J. Hazard. Mater.*, 2010, **174**, 47–53.
52 J.-F. Poggemann, A. Goβ, G. Heide, E. Rädlein and G. H. Frischat, *J. Non-Cryst. Solids*, 2001, **281**, 221–226.
53 X. Fang, S. Xiao, M. Shen, R. Guo, S. Wang and X. Shi, *New J. Chem.*, 2011, **35**, 360–368.
54 M. M. R. Khan, M. Ray and A. K. Guha, *Bioresour. Technol.*, 2011, **102**, 2394–2399.
55 A. Popat, S. B. Hartono, F. Stahr, J. Liu, S. Z. Qiao and G. Quing Max Lu, *Nanoscale*, 2011, **3**, 2801–2818.
56 S. Glastone, *Textbook of Physical Chemistry*, MacMillan Publishing Co, New York, 2nd edn, 1962, p. 1196.
57 A. Malek and S. Farooq, *AIChE J.*, 1996, **42**, 3191–3201.
58 P. Li, Y. F. Poon, W. Li, H.-Y. Zhu, S. H. Yeap, Y. Cao, X. Qi, C. Zhou, M. Lamrani, R. W. Beuerman, E.-T. Kang, Y. Mu, C. M. Li, M. W. Chang, S. S. J. Leong and M. B. Chan-Park, *Nat. Mater.*, 2010, **10**, 149–156.
59 M. Mahmoudi and V. Serpooshan, *ACS Nano*, 2012, **6**, 2656–2664.
60 H.-W. Liang, W.-J. Zhang, Y.-N. Ma, X. Cao, Q.-F. Guan, W.-P. Xu and S.-H. Yu, *ACS Nano*, 2011, **5**, 8148–8161.
61 Y. Wang, L. Cao, S. Guan, G. Shi, Q. Luo, L. Miao, I. Thistlethwaite, Z. Huang, J. Xu and J. Liu, *J. Mater. Chem.*, 2012, **22**, 2575–2581.
62 X. Li, J. Zhang, W. Xu, H. Jia, X. Wang, B. Yang, B. Zhao, B. Li and Y. Ozaki, *Langmuir*, 2003, **19**, 4285–4290.
63 J. S. Taurozzi, H. Arul, V. Z. Bosak, A. F. Burban, T. C. Voice, M. L. Bruenin and V. V. Tarabara, *J. Membr. Sci.*, 2008, **325**, 58–68.
64 L. Pratt and R. Kolter, *Mol. Microbiol.*, 1998, **30**, 285–293.
65 Y.-F. Huang, Y.-F. Wang and X.-P. Yan, *Environ. Sci. Technol.*, 2010, **44**, 7908–7913.
66 Y. S. Jeong, W.-K. Oh, S. Kim and J. Jang, *Biomaterials*, 2011, **32**, 7217–7225.
67 M. Tejamaya, I. Römer, R. C. Merrifield and J. R. Lead, *Environ. Sci. Technol.*, 2012, **46**, 7011–7017.
68 C. Levard, E. M. Hotze, G. V. Lowry and G. E. Brown Jr, *Environ. Sci. Technol.*, 2012, **46**, 6900–6914.
69 K. G. Scheckel, T. P. Luxton, A. M. El Badawy, C. A. Impellitteri and T. M. Tolaymat, *Environ. Sci. Technol.*, 2010, **44**, 1307–1312.
70 A. P. Gondikas, A. Morris, B. C. Reinsch, S. M. Marinakos, G. V. Lowry and H. Hsu-Kim, *Environ. Sci. Technol.*, 2012, **46**, 7037–7045.

